Chemical Engineering & Technology Research Article 1

Eduardo Poggio-Fraccari[1,2,*]
Fernando Mariño[2]
Concepción Herrera[1]
María Ángeles Larrubia-Vargas[1]
Luis Alemany[1]

Bi-reforming of Biogas for Hydrogen Production with Sulfur-Resistant Multimetallic Catalyst

A multimetallic sample, $NiCeSnRh/Al_2O_3$, was tested in methane reforming with a CH_4:H_2O:CO_2 molar ratio equal to 3:2:1. A very stable methane conversion with the time-on-stream was achieved during 20 h. Dimethyl sulfide served as a model sulfur molecule and a sulfurized sample was also tested. This achieved slightly lower conversion with a stable performance for more than 10 h and a minor but continuous decrease of its activity, after this period. The carbon dioxide conversion was always higher than the methane conversion in agreement with the lower H_2/CO ratio observed with respect to the theoretical value, 2/1, indicating the sulfur might block the active sites for H_2O activation. The analysis of the used catalysts showed graphitic and disordered carbon deposits.

Keywords: Biogas, Bi-reforming, Hydrogen production, Methane reforming, Multimetallic catalyst

Received: October 31, 2022; *revised:* December 28, 2022; *accepted:* January 27, 2023

DOI: 10.1002/ceat.202200525

This is an open access article under the terms of the Creative Commons Attribution-NonCommercial-NoDerivs License, which permits use and distribution in any medium, provided the original work is properly cited, the use is non-commercial and no modifications or adaptations are made.

Supporting Information available online

1 Introduction

Nowadays, the growing biogas production from agriculture wastes, underutilized resources, or sewage sludge favors the application of this raw material as a source of H_2 or syngas [1]. The composition of the biogas depends on the biomass source but it can be assumed that it is a wet mixture mainly composed of CH_4 and CO_2 [2]. Methane can be catalytically converted into a syngas stream by a reforming procedure. An alternative technology is the combined reforming also known as bi-reforming of methane (BRM), Eq. (1), a combination of the two well-known technologies, the steam methane reforming (SMR), Eq. (2), and the dry reforming of methane (DRM), Eq. (3). This approach is capable of obtaining a theoretical H_2/CO ratio equal to 2/1 which is suitable for Fischer-Tropsch synthesis [3, 4], but also minimizes the CO_2 emissions and coke deposition by methane decomposition according to Eqs. (4), and (5).

$$3CH_4 + 2H_2O + CO_2 \longrightarrow 4CO + 8H_2 \quad \Delta H = 659\ \text{kJ mol}^{-1} \tag{1}$$

$$CH_4 + H_2O \longrightarrow CO + 3H_2 \quad \Delta H = 206\ \text{kJ mol}^{-1} \tag{2}$$

$$CH_4 + CO_2 \longrightarrow 2CO + 2H_2 \quad \Delta H = 247\ \text{kJ mol}^{-1} \tag{3}$$

$$CH_4 \longrightarrow C + 2H_2 \quad \Delta H = 75\ \text{kJ mol}^{-1} \tag{4}$$

$$2CO \longrightarrow C + CO_2 \quad \Delta H = -172\ \text{kJ mol}^{-1} \tag{5}$$

The major downside of the biogas is that it carries some sulfur components such as H_2S, dimethyl sulfide (DMS), or methyl mercaptan [5], which are poisons for the conventional reforming catalysts. In the present work, DMS was used as a model molecule for this sulfur poison and a multimetallic sample catalyst was tested under BRM conditions of synthetic biogas $NiCeSnRh/Al_2O_3$.

Ni has been employed as a traditional component of methane reforming catalysts and more recently, the combination between Ni and ceria (Ce) has proven to be useful to enhance the activity of the catalysts and to carry out the SRM reaction at slightly lower temperatures due to the redox synergy between these components [6]. As well, an improved performance should also be expected due to the addition of Sn by two different features. Firstly, it was observed that the interaction between Ni-Sn improved the propensity to oxidize attached carbon atoms [7]. Secondly, it was concluded by

[1]Dr. Eduardo Poggio-Fraccari
https://orcid.org/0000-0002-9799-8967 (eduardopf@uma.es), Dr. Concepción Herrera, Dr. María Ángeles Larrubia-Vargas, Dr. Luis Alemany
Technology of Catalytic Processes PROCAT, Chemical Engineering Department, Faculty of Sciences, University of Malaga, Campus de Teatinos, 29071, Malaga, Spain.

[2]Dr. Eduardo Poggio-Fraccari, Dr. Fernando Mariño
Institute of Hydrogen Technologies and sustainable Energies ITHES (UBA-CONICET), Chemical Engineering Department, Faculty of Engineering, University of Buenos Aires, Ciudad Universitaria, 1428 Buenos Aires, Argentina.

 © 2023 The Authors. Chemical Engineering & Technology published by Wiley-VCH GmbH

Density Functional Theory (DFT) calculations that a Ni/Sn surface alloy exhibited enhanced sulfur resistance [8].

Otherwise, in a previous work it was reported that a Ni-Rh alloy improved the coke gasification of the monometallic Ni solids in the CO_2 and CO_2+H_2O reforming of methane [9]. In addition, this promoter may be also useful to improve the resistance to sulfur poisons present in the biogas stream. Ocsachoque et al. studied the deactivation by sulfur on these two active metals, Ni and Rh supported over Ce, by conducting a theoretical study by DFT. The authors have simulated the surface of the samples exposed to H_2S and demonstrated that Rh-supported Ce showed a higher tolerance to sulfur content in comparison with Ni/CeO_2 due to the fact that desorption of S–O species from Rh/CeO_2 is more favorable [10].

2 Experimental

A multimetallic $NiCeSnRh/Al_2O_3$ sample was obtained by simultaneous incipient wetness impregnation of the alumina support (S_{BET} = 246 m^2g^{-1}, V_p= 0.76 cm^3g^{-1}) with an aqueous solution of the chemical precursors: $Ni(NO_3)_2{\cdot}6H_2O$, $Ce(NO_3)_3{\cdot}6H_2O$, $Rh(NO_3){\cdot}xH_2O$, and an SnC_2O_4 solution in nitric acid in order to obtain the following nominal composition: 9 at nm^{-2} of Ni and 5 at nm^{-2} of Ce, Sn:Ni (1:1000 atomic ratio) and Rh:Ni (1:10 000 atomic ratio).

After the impregnation stage, the sample was kept in stagnant air at 90 °C overnight and then treated in air for 5 h (10 °C min^{-1}). This latter stage was followed by a reduction procedure at 700 °C (10 °C min^{-1}) during 20 min in 5 % of H_2 (N_2 as balance) with the aim of activating the sample. A poisoned sample was prepared by wetting a reduced catalyst with a DMS solution obtaining 0.2 wt % of DMS per catalysts mass. This solid was dried at 90 °C overnight and then tested under reaction conditions.

The catalyst was characterized by thermogravimetric analysis, Brunauer-Emmett-Teller (BET) isotherm, X-ray diffraction (XRD), Raman and X-ray Photoelectron Spectroscopy (XPS) equipment described elsewhere [4, 9].

The catalytic activity evaluation was conducted with a total flow of 100 mL min^{-1} (Gas Hourly Space Velocity (GHSV) = 3200 h^{-1}), 45 vol % CH_4, 30 vol % H_2O, 15 vol % CO_2 (N_2 balanced) representing a CH_4:H_2O:CO_2 ratio equal to 3:2:1. The conversion of CH_4 (Eq. (6)), and CO_2 (Eq. (7)), together with H_2/CO ratio (Eq. (8)) and carbon balance (Eq. (9)), were used to characterize the catalytic performance.

$$CH_4 \text{ conversion} : x_{CH_4} = \frac{F^{in}_{CH_4} - F^{out}_{CH_4}}{F^{in}_{CH_4}} \quad (6)$$

$$CO_2 \text{ conversion} : x_{CO_2} = \frac{F^{in}_{CO_2} - F^{out}_{CO_2}}{F^{in}_{CO_2}} \quad (7)$$

$$H_2/CO \text{ ratio} = \frac{F^{out}_{H_2}}{F^{out}_{CO}} \quad (8)$$

$$\text{Carbon balance} = \frac{F^{out}_{CH_4} + F^{out}_{CO_2} + F^{out}_{CO}}{F^{in}_{CH_4} + F^{in}_{CO_2}} \quad (9)$$

3 Results and Discussion

3.1 Characterization of Fresh and Reduced Samples

The thermal decomposition of the chemical precursors monitored by thermogravimetric analysis (TGA; see Fig. S1 in Supporting Information) showed a step at approximatively 220 °C in agreement with nitrate decomposition of Ni and Ce [11] while the corresponding to SnC_2O_4 is reported to occur close to 380 °C but the sample mass change was negligible due to the low content in the solid [12] and was unnoticed. In addition to the original catalyst, two extra samples were also characterized, one obtained after the reduction procedure with H_2 (activation stage) and another reduced solid wetted with a saturated solution of DMS producing an ex-situ poisoned catalyst, hereafter denoted as sulfurized sample. The surface area decreased by 17 % after the reduction from 150 to 124 m^2g^{-1}, suggesting a probable loss of active surface by agglomeration of crystallites; see Tab. 1.

The XRD pattern of the fresh solid showed different crystalline phases as indicated in Fig. 1. Sn or Rh species were not observed. The lattice parameter of the fluorite phase was slightly lower than the reported value for a similar Ce catalyst

Table 1. Summary of characterization results of XRD, Raman, and XPS for $NiCeSnRh/Al_2O_3$ under different studied conditions. The used samples correspond to 20 h in reaction stream at 700 °C.

Sample	$a_{fluorite}$ [nm]	$d_{fluorite}$ [nm]	a_{Ni^0} [nm]	d_{Ni^0} [nm]	I_G/I_D	Ce^{3+}/Ce [%]	Ni/Ce
Fresh	0.5401	5.4	0.4156 (NiO)	8.5 (NiO)	–	22	1.5
Reduced	0.5411	5.9	0.3521	5.9	–	34	0.7
Reduced-sulfurized[a)]	0.5409	4.6	0.3519	4.1	–	38	1.0
Used	0.5422	5.6	0.3506	11.2	0.47	ND	ND
Used-sulfurized*	0.5400	8.5	0.3521	13.3	0.72	ND	ND

[a)] 0.2 wt % of DMS added ex-situ.

 © 2023 The Authors. Chemical Engineering & Technology published by Wiley-VCH GmbH

15214125, 0, Downloaded from https://onlinelibrary.wiley.com/doi/10.1002/ceat.202200525 by Chua-Consorcio De Bibliotecas, Wiley Online Library on [05/05/2023]. See the Terms and Conditions (https://onlinelibrary.wiley.com/terms-and-conditions) on Wiley Online Library for rules of use; OA articles are governed by the applicable Creative Commons License

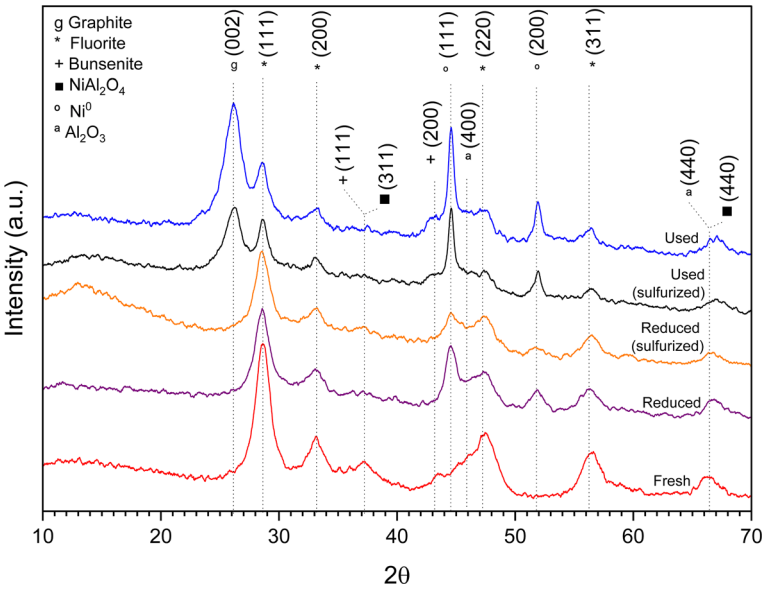

Figure 1. X-ray diffraction patterns of fresh, reduced, and used samples. CeO_2 (PDF#43-1002), NiO (PDF#47-1049), $NiAl_2O_4$ (PDF#10-0339), Ni^0 (PDF#04-0850), Al_2O_3 (PDF#10-0425).

calcined at the same temperature range, which might indicate a possible replacement of the host Ce^{4+} ions of the lattice by other smaller such as Ni^{2+}, Sn^{4+} or Rh^{4+} [13]; see Tab. 1. Otherwise, the lattice parameter of bunsenite phase showed a value very close to the theoretical reported in the PDF chart, 0.4177 nm.

The crystallite size of fluorite and bunsenite species were estimated by the Scherrer equation. After the activation stage, an increase of the crystallite size of the fluorite particles for this reduced sample was observed in conformity with the lower BET surface area measured. For this sample, an expansion of the unit cell was found as it was expected by the reduction of Ce^{4+} ions to the larger size Ce^{3+} in agreement with XPS results. The main peak of the $NiAl_2O_4$ phase could not be identified in this reduced sample implying that no crystalline phase is present after the activation procedure. By analyzing the pattern of the sulfurized solid it can be seen that the lattice parameters of the fluorite and cubic phase of the metallic nickel remained almost unchanged when they are compared with the reduced sample suggesting that no major changes were observed in the solid by the impregnation with the sulfur compound. The analysis of these used samples will be detailed later in the manuscript.

Raman spectroscopy was used to characterize the catalysts (Fig. 2). The original solid showed a peak at 458 cm^{-1}, ascribed to the well-known F2g vibrational mode of Ce^{4+} cations [14], while the broad band between 550 and 650 cm^{-1} may indicate the presence of oxygen vacancies [15, 16] as well as the interaction of Ni and Ce by Ni–O–Ce species [17]. The reduced sample presented much less intense bands as it was expected after H_2 exposure [18]. The peak previously found at 636 cm^{-1} in the fresh sample was not observed in the reduced one and apparently might be merged as a single peak close to 600 cm^{-1}. It is worth mentioning that the band of the most probable sulfur compound according to XPS analysis, $Ce_2(SO_4)_3$ close to 1100 cm^{-1}, was not found [19]. The deconvolution procedure delivered different peaks, one corresponding to the previously mentioned F2g band (450–460 cm^{-1}), another ascribed to the O vacancies (close to 554 cm^{-1}) in agreement with the reduced and clean sample, but the remaining at 615 cm^{-1} is not correlated to any previously observed, which might indicate oxygen vacancies due to a possible Ce-S-O interaction.

The main spectra of the components Ce3d, Ni2p, Sn3d, including the S2p region (poison), and the adventitious carbon C1s are reported in the Supporting Information, Fig. S2. In all Ni2p spectra, two doublets and two satellites were identified in agreement with the literature [20]. Specifically, both reduced samples, clean and sulfurized, presented a peak close to 852 eV indicating a fraction of reduced Ni. The analysis of the Ce3d spectrum showed a high content of trivalent ions in the fresh sample in agreement with the intense bands in the Raman spectra between 500–700 cm^{-1} (Tab. 1). In the sulfurized solid the highest value of Ce^{3+} ions was found indicating a clear effect of the DMS attached on the surface of the catalyst. This is presumably due to the formation of Ce sulfates(III) as it was reported in the literature by the oxidation of the sulfide anion with the Ce^{4+} ions [21, 22]. In fact, the S2p spectrum showed a broad band with a doublet at 168.5 and 169.8 eV ruling out the presence of inorganic sulfides (161–162 eV), adsorbed H_2S (170.7 eV) or CH_3SH (170 eV) [23].

Other possible containing compounds are dimethyl sulfide (169.5 eV) and dimethyl disulfide (169.8 eV) [24]. However, both fitted peaks (after charge correction) are located almost at 1 eV lower binding energy in the sample in comparison with the reference values. Tin, Ce, and Ni sulfates present signals in the range of 167.9–169.7 eV, according to the NIST database, which are in a better agreement with the fitted peaks [25]. As a consequence, it might be possible that different sulfates were formed after the exposure of the sample to the DMS including the well-known $Ce_2(SO_4)_3$ as it was theoretically predicted by Density Functional Theory (DTF) [26].

3.2 Activity Performance Evaluation

A preliminary test of the clean sample indicated that methane conversion was noticeable for temperatures higher than 625 °C. Then, the ex-situ sulfurized solid was tested in the same range (625–700 °C) with the aim of understanding the effect of the poison. This sample was used as an attempt to split different possible involved phenomena, by studying the sulfur interaction with the active sites in the presence of gaseous reactants avoiding the probable continuous change in the catalysts surface by a constant feed including sulfur. This latter approach may hinder the analysis carried out to shed light on the deactivation of the sample. The results of the light-off curves are reported in Fig. 3 along with the equilibrium composition calculated by the minimization of the Gibbs free energy [27] including the solid coke species following the procedure reported elsewhere [28].

 © 2023 The Authors. Chemical Engineering & Technology published by Wiley-VCH GmbH

15214125, 0, Downloaded from https://onlinelibrary.wiley.com/doi/10.1002/ceat.202200525 by Chua-Consorcio De Bibliotecas, Wiley Online Library on [05/05/2023]. See the Terms and Conditions (https://onlinelibrary.wiley.com/terms-and-conditions) on Wiley Online Library for rules of use; OA articles are governed by the applicable Creative Commons License

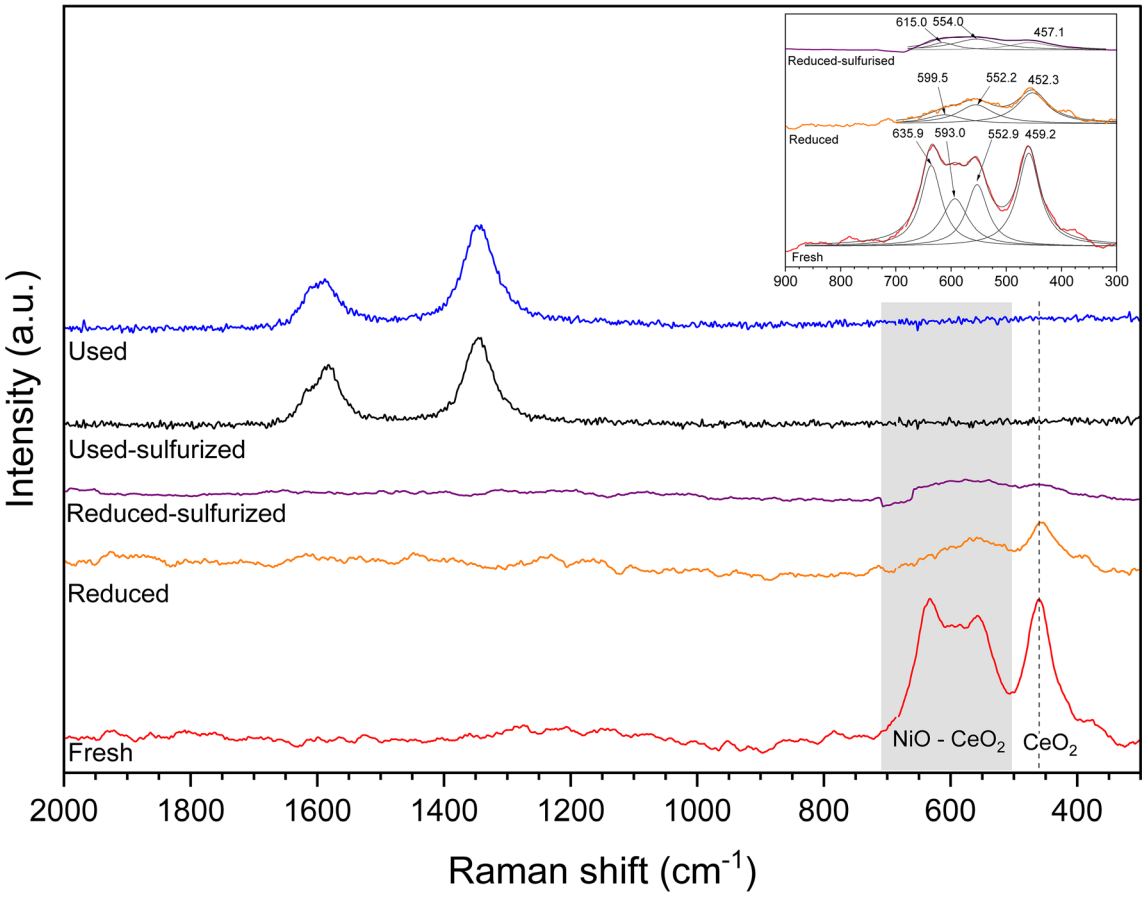

Figure 2. Raman spectra of fresh and reduced samples of multimetallic NiCeSnRh/Al_2O_3.

It is worth mentioning that neither DMS nor any sulfur species were included in the thermodynamic equilibrium study due to it was assumed that sulfur was strongly attached to the surface and methyl groups were decomposed during the drying step in the poisoning procedure in agreement with XPS results. Theoretical methane conversion is always higher for the studied temperature range when carbon deposition is allowed, probably by the occurrence of CH_4 decomposition that further increases methane conversion, or by the extent of the Boudouard reaction (Eq. (4)), which favors the occurrence of BRM due to the consumption of CO (Eq. (5)). CO_2 equilibrium conversion also increases with the temperature (Fig. 3b), and the calculated values are slightly higher when carbon deposits are considered, suggesting that carbon atoms may also be distributed in a new phase.

On the other hand, the H_2/CO ratio is markedly increased by lowering the temperature of the reactor (Fig. 3c), in agreement with the simulation results of Matus et al. [29]. This is due to the activation of the water-gas shift reaction that consumes 1 mole of CO to form an additional H_2 mole. What is more, if carbon is allowed in the calculus, the H_2/CO ratio is further increased by the possible decomposition of methane providing additional H_2. The theoretical ratio of carbon-containing molecules between the inlet and the outlet of the reactor (Fig. 3d) showed that the values of the equilibrium curve including the carbon deposits are increased, i.e., the coke yield decreases with temperature [30] implying that H_2O and CO_2 gasification reactions of solid coke are enhanced in this range.

The experimental methane conversion increased with the temperature as it was expected for this endothermic reaction and, in comparison, the sulfurized sample showed lower values suggesting that some active sites may be unavailable to the reaction after the exposure to the DMS. This is probably by the generation of sulfates as it was suggested by the analysis of the XPS and Raman spectra. In the case of the CO_2 conversion, both samples followed the same trend with the temperature, but the poisoned sample presented slightly lower values instead of the appreciable difference found for CH_4 conversion, except for the highest temperature when both values of fresh and sulfurized samples were quite similar.

In line with this trend, a moderate increase for the H_2/CO ratio with the reaction temperature can be observed, achieving at 700 °C a ratio very close to the theoretical value H_2/CO = 2 according to Eq. (5), but presenting lower values for temperatures lower than 700 °C in agreement with the theoretical ratio H_2/CO = 1 of the dry methane reforming reaction (Eq. (2)). In summary, the sulfur presence induced a lower CH_4 conversion with almost unchanged CO_2 conversion, and a concomitant decrease of H_2/CO. Therefore, it seems that the active sites capable of performing the H_2O activation are presumably blocked by the sulfur presence hindering the SMR reaction.

 © 2023 The Authors. Chemical Engineering & Technology published by Wiley-VCH GmbH

15214125, 0, Downloaded from https://onlinelibrary.wiley.com/doi/10.1002/ceat.202200525 by Cbua-Consorcio De Bibliotecas, Wiley Online Library on [05/05/2023]. See the Terms and Conditions (https://onlinelibrary.wiley.com/terms-and-conditions) on Wiley Online Library for rules of use; OA articles are governed by the applicable Creative Commons License

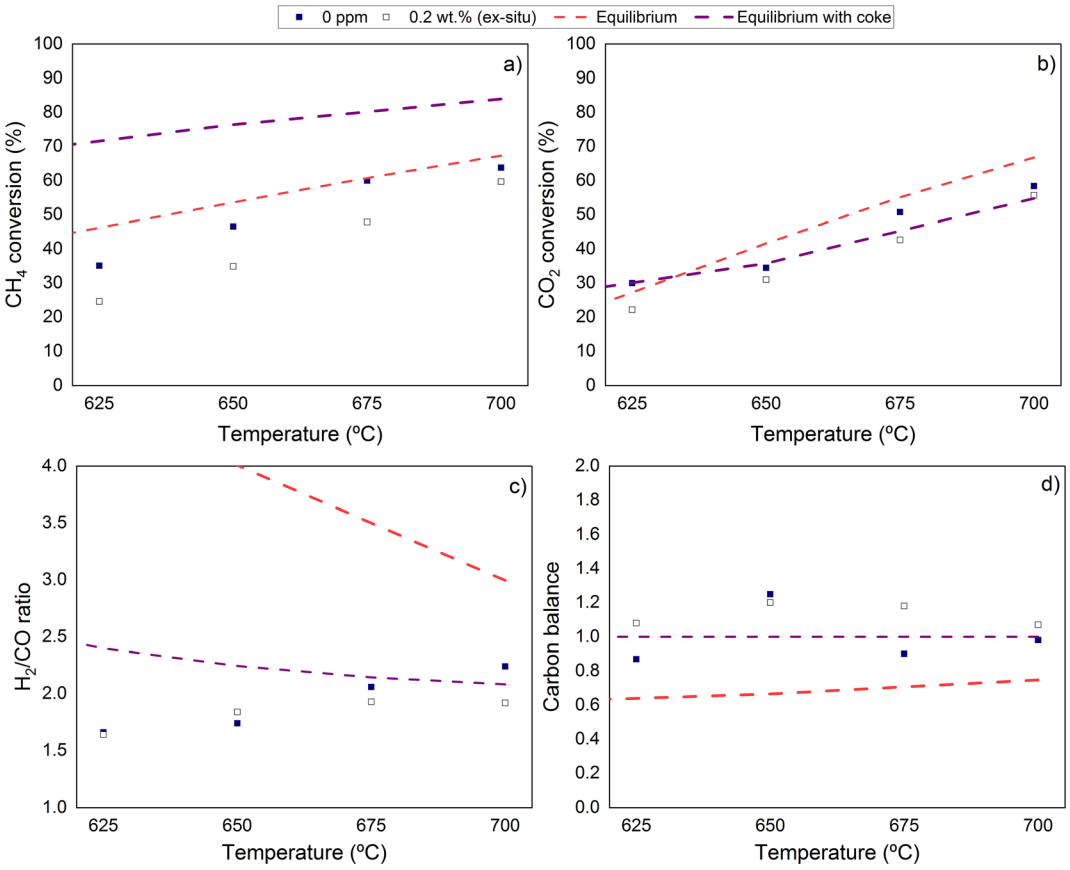

Figure 3. Catalytic performance results versus temperature for clean sample (0 ppm) and poisoned sample (0.2 wt % ex-situ). (a) CH_4 conversion, (b) CO_2 conversion, (c) H_2/CO ratio, (d) carbon ratio. Thermodynamic equilibrium conditions omitting and including coke deposition are plotted with dashed and dotted lines, respectively.

Otherwise, the ratio of carbon-containing components between the inlet and the outlet of the reactor showed scattered values around the calculated equilibrium since this parameter involves several magnitudes (molar fractions of different components). It is expected to have a certain dispersion due to the error propagation during calculus in agreement with other authors in the literature [31]. However, the processes of carbon deposition and gasification may occur during the test as it was evidenced by the post-run analysis and the equilibrium calculus.

A long-term run was carried out and the results are reported in Fig. 4 together with the equilibrium values for the sake of clarity. The performance of both samples presented two different stages with the evolution of the variable time-on-stream, hereafter called TOS. Firstly, an induction period was observed during the first two hours of continuous exposition to the gas mixture, characterized by a clear change of all the reaction parameters and secondly, a stage marked by a very stable response of the clean solid and a moderate decrease of the sulfurized sample. Regarding the clean catalysts, the observed prominent initial values may be decreased by a combination of factors which involve changes of the different active sites of the multimetallic catalyst.

On the one hand, the loss of active area of Ni particles was evidenced by the increase of the crystallite size and became twice as the corresponding value of the reduced sample (Tab. 1), owing to the exposure to the H_2O stream as it was also observed for Ni/Ce catalysts [32]. On the other hand, the decrease in the catalytic activity of the sample was also due to a quick coke formation on the surface of the solid as it was indicated by the results of the thermodynamic calculus and clearly observed by the Raman spectra presented in Fig. 2.

In fact, the coke content was so relevant that almost 40 wt % of the spent recovered catalyst was coke. This will be detailed in the next section involving a post-run study. By analyzing the results obtained from the second stage of the long-term run for the multimetallic catalyst, it can be seen that the achieved CH_4 and CO_2 conversion values after 20 h were 55 % and 45 %, respectively, and the H_2/CO ratio was very close to the theoretical 2/1 suggesting that a bi-reforming reaction has taken place during the entire experiment.

These results imply that the proposed catalyst is capable of successfully performing the reaction even in the presence of coke deposits and the sintering of the Ni active phase after an induction period. By comparison with other samples reported in the literature under similar reaction conditions (Tab. 2), it

 © 2023 The Authors. Chemical Engineering & Technology published by Wiley-VCH GmbH

15214125, 0, Downloaded from https://onlinelibrary.wiley.com/doi/10.1002/ceat.202200525 by Cbua-Consorcio De Bibliotecas, Wiley Online Library on [05/05/2023]. See the Terms and Conditions (https://onlinelibrary.wiley.com/terms-and-conditions) on Wiley Online Library for rules of use; OA articles are governed by the applicable Creative Commons License

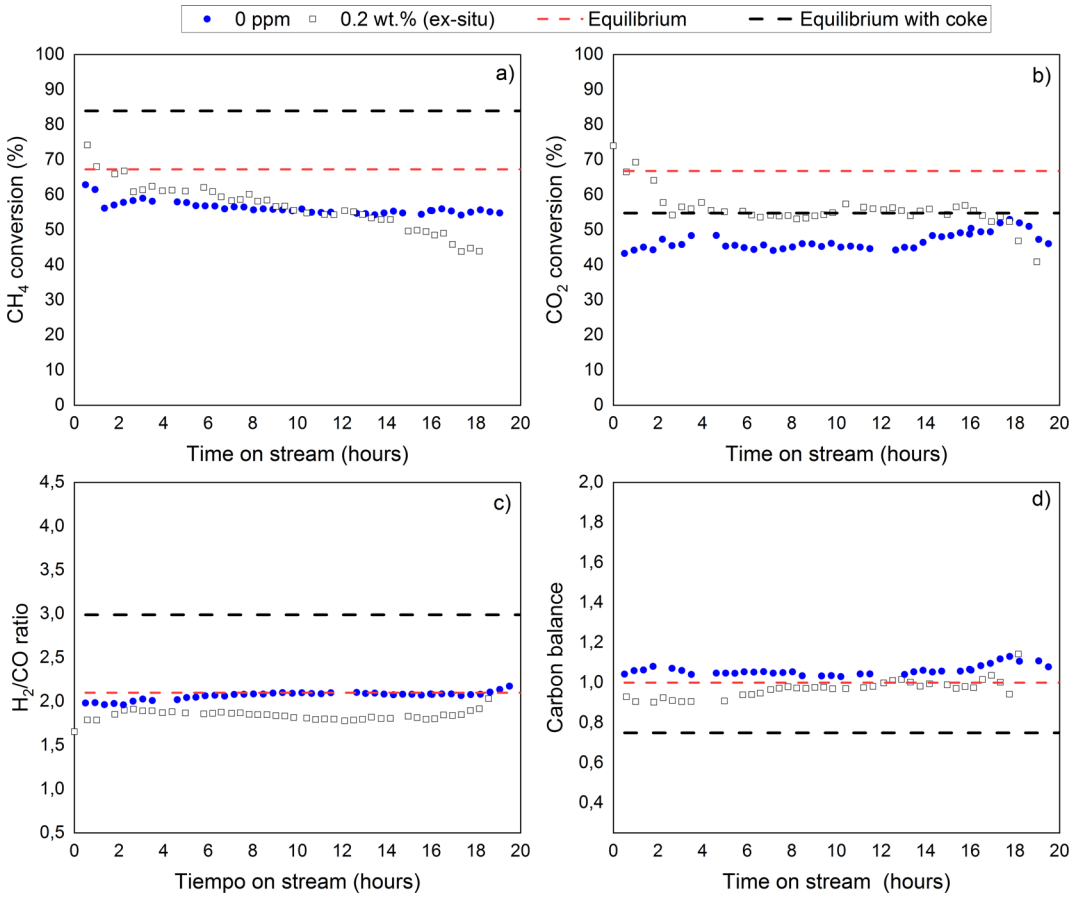

Figure 4. Stability analysis of the samples, clean and poisoned ex-situ, under BRM conditions at 700 °C. (a) CH_4 conversion, (b) CO_2 conversion, (c) H_2/CO ratio, d) carbon balance. Equilibrium conditions omitting and including C deposition are plotted with dashed and dotted lines, respectively.

Table 2. Summary of catalytic performance of several Ni-containing catalysts for BRM stability test.

Catalyst	T [°C]	GHSV [h^{-1}]	CH_4:H_2O:CO_2 molar ratio	TOS [h]	x_{CH_4} [%]	x_{CO_2} [%]	H_2/CO ratio	Ref.
NiCeSnRh/Al_2O_3	700	3200	3:2:1	20	55	45	2	This work
Ni/Al_2O_3	700	13650	1:0.8:0.48	6	75	–	–	1
NiO/CeO_2	700	≈ 1900	3:2.4:1.2	30	75	78	–	33
Co-Pt-Zr-La/Al_2O_3	700	1500	1:1:1	100	99	80	1.5	41
Ni/CeO_2	700	≈ 1270	3:2.4:1.2	30	75	75	–	42
Co-Pt/Al_2O_3(Zr)	700	1000	1:0.2:1	50	100	100	1.6	43
Ni/$CeZrO_2$	800	≈ 11 250	1:0.8:0.4	20	50	–	–	44
NiRh/Al_2O_3	700	6000	3:2:1	14	40	50	0.75	45

can be found that methane and carbon dioxide conversions were acceptable in line with the moderate GHSV employed, while other noble metal-based catalysts were tested at half or even a third of our GHSV [41, 43].

In addition, the achieved H_2/CO ratio very close to 2 was higher than others indicating that the catalyst and the reaction conditions chosen were convenient to produce syngas. Finally, the stability was evaluated during a 20-h TOS pointing out that this is very promising catalyst comparable with those reported in the literature. A lengthy summary of BRM stability results including different catalysts supports can be found elsewhere [33, 34]. Otherwise, to the best of our knowledge, the published

 © 2023 The Authors. Chemical Engineering & Technology published by Wiley-VCH GmbH

15214125, 0, Downloaded from https://onlinelibrary.wiley.com/doi/10.1002/ceat.202200525 by Cbua-Consorcio De Bibliotecas, Wiley Online Library on [05/05/2023]. See the Terms and Conditions (https://onlinelibrary.wiley.com/terms-and-conditions) on Wiley Online Library for rules of use; OA articles are governed by the applicable Creative Commons License

works dealing with sulfur poisoning in methane reforming are very scarce, normally constrained to steam or dry reforming and involving noble metals-based catalysts [35, 36].

The catalytic performance of the sulfurized NiCeSnRh/Al_2O_3 sample also presented an induction period with a marked decrease in the performance. According to the results observed for the second period, the methane conversion showed a noticeable decrease while the CO_2 conversion presented more stable values, simultaneously with a H_2/CO ratio close to 1.8, lower than theoretically expected for BRM H_2/CO = 2/1. Since the BRM is a linear combination of SMR and DMR, Eq. (1) =2Eq. (2)+Eq. (3), the observed trend in both analized conversions suggest that the SMR was hindered in agreement with the lower H_2/CO ratio found.

In addition, the presence of the poison caused the sintering of the sample since the crystallite sizes of the fluorite and the metallic Ni have been enlarged (see Tab. 1). As a consequence, the metal support interface was shrunk, severely affecting the amount of available active sites for H_2O splitting as it was reported in the literature by a DFT study conducted for a Ni-CeO_2 solid [37]. Otherwise, in the case of the DRM reaction, the most favorable sites for CO_2 activation were identified as oxygen vacancies located at the interface of Ni-Ce as well as at the support (with further migration of the labile oxygen) [38].

In conclusion, the attached sulfur had a more severe effect in the SMR reaction. These observations are in agreement with the common reaction mechanism reported for SMR and DRM for Ni/CeO_2 in which Ce has an active role in the catalytic performance [39, 40]. Finally, at the end of the run (TOS > 15 h), a simultaneous decrease of the CH_4 and CO_2 conversions was observed suggesting that the active sites had been partially blocking by coke deposits. This is a noticeable difference with the stable performance of the original sample (without sulfur) that also presented a considerable amount of coke deposit (as it will be discussed below), indicating a possible synergy between sulfur and coke deposition as deactivation mechanisms. With the purpose of conducting an thorough analysis of the causes of the deactivation, the used samples were studied by XRD, Raman, and TGA.

3.3 Evaluation of Used Samples

Both spent catalysts were analyzed after the long-term reaction with TOS = 20 h. As it can be seen in the XRD patterns preented in Fig. 1, a clear graphite signal was found in both catalysts, in agreement with the Raman spectra shown Fig. 2. In addition, fluorite and metallic Ni signals were identified. By comparing these with the corresponding one of the reduced sample, a change in the intensity and the width of peaks is observed indicating a higher crystallite size due to the exposure to reaction conditions. As a result, a clear reduction in metallic surface area can be inferred, which is more marked in the case of the sulfurized sample as it was stated before; see values in Tab. 1. By analyzing the obtained values for the lattice parameter of the fluorite, a higher value for the used sample with respect to the reduced solid can be stated, suggesting an expansion probably by a higher content of Ce^{3+}. Otherwise, the used-sulfurized catalyst showed a lower value in comparison with the reduced-sulfurized one, demonstrating a shrinkage due to the incorporation of smaller cations into the unit cell which might be carbon or sulfur.

Regarding the lattice parameter of the metallic Ni, no appreciable change was found for this sulfurized sample but a contraction was observed, which might also be due to a Ni–C interaction. This will be further studied. Raman spectroscopy is useful to identify coke formation after the exposure of the sample to reaction conditions. In order to investigate the spatial homogeneity of carbon deposits, several spectra were recorded at different locations. The results indicate minor changes between different spots and the spectra with the most prominent carbon signals are reported in Fig. 2. Two marked signals were observed at 1342–1348 cm^{-1} and 1587–1595 cm^{-1} ranges. These are associated to different carbon species probably formed by the Boudouard reaction and/or CH_4 decomposition. At a lower shift the D-band can be found which is related to the presence of disordered carbon, whilst the second is known as G-band addressed to graphitic carbon [42].

The type of carbonaceous species strongly determines the possibility of sample reactivation by conducting a soft or harsh treatment. The most unreactive is the graphitic carbon followed by amorphous carbon, and then the carbidic [46]. Some authors claimed that the D-band is associated with a mixture of carbidic and amorphous carbon [47]. However, other authors argued that in the presence of carbon nanotubes the D-band may indicate defects in the nanotube walls and the amorphous carbon may be identified by a very broad peak beneath the D- and G-peaks, practically absent in the studied samples of the present work. Also, the G-band of carbon is an in-plane ring stretching mode characteristic of graphite (1575 cm^{-1}), multiwalled carbon nanotubes (1580 cm^{-1}) or graphite clusters (1600 cm^{-1}) [48].

The ratio of the intensities of the D and G bands was used to characterize the degree of graphitization of the coke deposit, and therefore, the feasibility of sample reactivation with a soft treatment, i.e., a low D and G band intensities (I_G/I_D) ratio is considered beneficial. The sample poisoned ex-situ with DMS presented a value close to 0.5 in contrast with the 0.7 of the clean catalyst (Tab. 1). As a consequence, the sulfur content in the sample favors the formation of the graphitic carbon as it was also observed by Frontera et al. in the presence of H_2S during ethanol steam reforming at 700 °C [49]. However, the amount of coke present is less in the sulfurized sample in comparison as it was calculated by the TGA, with 41 % for the sulfurized sample and 48 % for the original catalyst (Fig. 3). This suggests that the attached sulfur to the surface of the solid may hinder the carbon deposition during the reaction. The same behavior is reported for the Ni-based catalysts of the steam crackers.

The usual procedure carried out is the sulfurization with dimethyl disulfide (DMDS) of the catalytic solid with the objective of minimize the material coking tendency by inducing the passivation of active metal by a strong attach of the sulfur [50, 51]. The Differential Thermogravimetric analysis (DTG) profiles of used samples (Fig. 5) in the long-term run analysis showed two clear peaks at 525 °C and 640–660 °C indicating two different carbon species present. The first one, oxidized at lower temperature, is normally ascribed to amorphous carbon while the second is related to graphitic carbon [52] in agreement with the findings of Raman analysis (Fig. 2). In summary, it is expected that the catalyst could be reactivated in a

 © 2023 The Authors. Chemical Engineering & Technology published by Wiley-VCH GmbH

15214125, 0, Downloaded from https://onlinelibrary.wiley.com/doi/10.1002/ceat.202200525 by Chua-Consorcio De Bibliotecas, Wiley Online Library on [05/05/2023]. See the Terms and Conditions (https://onlinelibrary.wiley.com/terms-and-conditions) on Wiley Online Library for rules of use; OA articles are governed by the applicable Creative Commons License

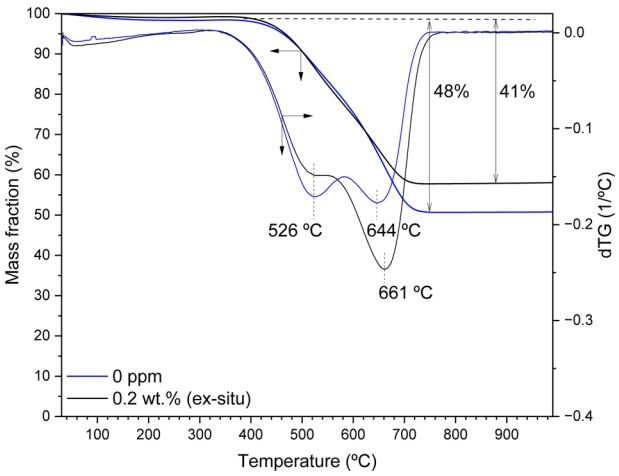

Figure 5. Temperature-programmed oxidation of the used samples with 4 % O_2 in N_2 (100 mL min^{-1}) and 10 °C min^{-1}.

soft oxidation treatment with steam instead of the common technique employing diluted oxygen, because most of the present coke is disordered carbon [53].

4 Conclusions

The studied multimetallic sample proved to be useful to convert synthetic biogas into a syngas stream. The light-off curves demonstrated that it is more convenient to operate at the highest temperature. The results of the long-term run evidenced a stable performance for almost 20 h. Actually, the achieved performance was comparable with previous Ni-based catalysts reported in the literature under clean conditions.

The DMS incorporation caused the deactivation of the sample by a strong attach to the surface owing to the presence of sulfates probably cerium sulfate. This compound has induced the sintering of the sample decreasing the Ni–Ce interface hindering the SMR reaction. In addition, the clean and the sulfurized samples showed a relevant content of coke after the run. As a consequence, it was assumed that the main effect of the attached sulfur to the sample surface was the deactivation of the solid by blocking of the actives located at the Ni–Ce interface and inducing the formation of graphitic carbon. However, it is expected that a soft reactivation treatment will be capable of regenerating the solid removing the disordered coke.

Supporting Information

Supporting Information for this article can be found under DOI: https://doi.org/10.1002/ceat.202200525.

Acknowledgment

Funding for open access charge: Universidad de Málaga/CBUA.

The authors have declared no conflict of interest.

Symbols used

F_j^{in}	[mol s^{-1}]	inlet molar flow, *j*: CH_4, H_2O, CO_2, CO, H_2
F_j^{out}	[mol s^{-1}]	outlet molar flow, *j*: CH_4, H_2O, CO_2, CO, H_2

Abbreviations

BET	Brunauer-Emmett-Teller
BRM	bi-reforming of methane
DFT	Density Functional Theory
DMS	dimethyl sulfide
DTG	Differential Thermogravimetric analysis
GHSV	Gas Hourly Space Velocity
I_G/I_D	Intensity ratio of G and D Raman bands
SMR	steam methane reforming
TGA	thermogravimetric analysis
TOS	time-on-stream
XRD	X-ray diffraction

References

[1] M. Dan, M. Mihet, G. Borodi, M. Lazar, *Catal. Today* **2021**, *366*, 87–96. DOI: https://doi.org/10.1016/j.cattod.2020.09.014
[2] A. Calbry-Muzyk, H. Madi, F. Rüsch-Pfun, M. Gandigli, S. Biollaz, *Renewable Energy* **2022**, *181*, 1000–1007. DOI: https://doi.org/10.1016/j.renene.2021.09.100
[3] A. S. Farooqi, M. Yusuf, N. A. Zabidi, R. Saidur, K. Sanaullah, A. Farooqi, A. Khan, B. Abdullah, *Int. J. Hydrogen Energy* **2021**, *46*, 31024–31040. DOI: https://doi.org/10.1016/j.ijhydene.2021.01.049
[4] M. García-Diéguez, I. Pieta, M. C. Herrera, M. A. Larrubia, L. J. Alemany, *J. Catal.* **2010**, *270*, 136–145. DOI: https://doi.org/10.1016/j.jcat.2009.12.010
[5] S. Rasi, A. Vaijanen, J. Rintala, *Energy* **2007**, *32*, 1375–1380. DOI: https://doi.org/10.1016/j.energy.2006.10.018
[6] I. Iglesias, G. Baronetti, L. J. Alemany, F. J. Mariño, *Int. J. Hydrogen Energy* **2019**, *44*, 3688–3680. DOI: https://doi.org/10.1016/j.ijhydene.2018.12.112
[7] E. Nikolla, J. Schwank, S. Linic, *J. Catal.* **2009**, *263*, 220–227. DOI: https://doi.org/10.1016/j.jcat.2009.02.006
[8] M. Rangan, M. Yung, W. Medlin, *J. Catal.* **2011**, *282*, 249–257. DOI: https://doi.org/10.1016/j.jcat.2011.06.009
[9] M. García-Diéguez, I. Pieta, M. C. Herrera, M. A. Larrubia, L. J. Alemany, *Catal. Today* **2011**, *172*, 136–142. DOI: https://doi.org/10.1016/j.cattod.2011.02.012
[10] M. A. Ocsachoque, J. I. Russman, B. L. Irigoyen, D. Gazzoli, M. G. González, *Mater. Chem. Phys.* **2016**, *172*, 69–76. DOI: https://doi.org/10.1016/j.matchemphys.2015.12.062
[11] A. Holdsworth, A. Horrocks, B. Kandola, D. Price, *Polym. Degrad. Stabil.* **2014**, *110*, 290–297. DOI: https://doi.org/10.1016/j.polymdegradstab.2014.09.007
[12] E. A. Poggio, M. Moreno, M. Jobbagy, M. A. Laborde, F. J. Mariño, G. Baronetti, *Int. J. Hydrogen Energy* **2011**, *36*, 15899–15905. DOI: https://doi.org/10.1016/j.ijhydene.2011.09.026

 © 2023 The Authors. Chemical Engineering & Technology published by Wiley-VCH GmbH

15214125, 0, Downloaded from https://onlinelibrary.wiley.com/doi/10.1002/ceat.202200525 by Cbua-Consorcio De Bibliotecas, Wiley Online Library on [05/05/2023]. See the Terms and Conditions (https://onlinelibrary.wiley.com/terms-and-conditions) on Wiley Online Library for rules of use; OA articles are governed by the applicable Creative Commons License

[13] E. A. Poggio-Fraccari, B. L. Irigoyen, G. Baronetti, F. J. Mariño, *Appl. Catal., A* **2014**, *485*, 123–132. DOI: https://doi.org/10.1016/j.apcata.2014.07.040
[14] J. McBride, K. Hass, D. Poindexter, H. Weber, *Appl. Phys.* **1994**, *76*, 2435–2441. DOI: https://doi.org/10.1063/1.357593
[15] C. Alvarez-Galvan, J. Martínez, M. Capel-Sanchez, L. Pascual, J. Alonso, *Adv. Sustainable Syst.* **2021**, *5*, 2100029–2100039. DOI: https://doi.org/10.1002/adsu.202100029
[16] K. Tang, W. Liu, J. Li, J. Guo, J. Zhang, S. Wang, S. Niu, Y. Yang, *Appl. Mater. Interfaces* **2015**, *7*, 26839–26849. DOI: https://doi.org/10.1021/acsami.5b09110
[17] C. Xian, S. Wang, C. Wei, C. Sun, H. Li, S. Chan, L. Chen, *Chin. J. Catal.* **2013**, *34*, 305–312. DOI: https://doi.org/10.1016/S1872-2067(11)60466-X
[18] M. Louie, A. Bell, *J. Am. Chem. Soc.* **2013**, *135*, 12329–12337. DOI: https://doi.org/10.1021/ja405351s
[19] Z. Li, J. Chen, M. Liang, L. Li, J. Zhang, W. Duan, J. Wen, H. Wang, M. Liu, Q. Zhang, J. Chen, P. Ning, *Catal. Lett.* **2022**, *152*, 2729–2737. DOI: https://doi.org/10.1007/s10562-021-03846-8
[20] *Handbook of X-ray Photoelectron Spectroscopy* (Eds: C. Wagner, W. Riggs, L. David, J. Moulder, G. Muilenberg), Perkin Elmer Corp., Eden Prairie, MN **1979**.
[21] D. He, Y. Zhang, W. Mei, Y. Jiang, *Energy Fuels* **2020**, *34*, 4822–4827. DOI: https://doi.org/10.1021/acs.energyfuels.9b03312
[22] Q. Zhou, X. Tao, G. Di, Y. Shang, P. Lu, G. Xu, M. Liu, Y. Zheng, *Energy Fuels* **2021**, *35*, 5101–5109. DOI: https://doi.org/10.1021/acs.energyfuels.0c04208
[23] Y. Duan, L. Pirolli, A. Teplyakov, *Sens. Actuators B* **2016**, *235*, 213–221. DOI: https://doi.org/10.1016/j.snb.2016.05.014
[24] T. Carroll, D. Ji, D. McLaren, T. Thomas, L. Saethre, *J. Electron. Spectrosc. Relat. Phenom.* **1987**, *42*, 281–284. DOI: https://doi.org/10.1016/0368-2048(87)80039-7
[25] https://srdata.nist.gov/xps/Default.aspx
[26] J. Li, C. Zhang, Q. Li, T. Gao, S. Yu, P. Tang, Q. Fang, Q. Chen, *Chem. Eng. Sci.* **2022**, *251*, 117438–117456. DOI: https://doi.org/10.1016/j.ces.2022.1174358
[27] R. Wess, F. J. Nores-Pondal, M. A. Laborde, P. D. Giunta, *Chem. Eng. Sci.* **2015**, *134*, 86–95. DOI: https://doi.org/10.1016/j.ces.2015.04.002
[28] C. Graschinsky, P. D. Giunta, N. E. Amadeo, M. A. Laborde, *Int. J. Hydrogen Energy* **2012**, *37*, 10118–10124. DOI: https://doi.org/10.1016/j.ijhydene.2012.01.182
[29] E. Matus, O. Sukhova, I. Ismagilov, M. Kerzhentsev, L. Li, Z. Ismagilov, *J. Phys. Conf. Ser.* **2021**, *1749*, 012023. DOI: https://doi.org/10.1088/1742-6596/1749/1/012023
[30] W. Jang, D. Jeong, J. Shim, H. Kim, H. Roh, I. Son, S. Lee, *Appl. Energy* **2016**, *173*, 80–91. DOI: https://doi.org/10.1016/j.apenergy.2016.04.006
[31] A. Brush, E. Evans, G. Mullen, K. Jarvis, C. Mullins, *Fuel Process. Technol.* **2016**, *153*, 111–120. DOI: https://doi.org/10.1016/j.fuproc.2016.07.012
[32] M. Shakouri, Y. Hu, R. Lehoux, H. Wang, *Can. J. Chem. Eng.* **2011**, *99*, 153–165. DOI: https://doi.org/10.1002/cjce.23828
[33] L. Loc, P. Phuong, D. Putthea, N. Tri, N. Van, H. Cuong, *Int. J. Nanotechnol.* **2018**, *15*, 968–982. DOI: https://doi.org/10.1504/IJNT.2018.099935
[34] U. Mohanty, M. Ali, M. Azhar, A. Al-Yaseri, A. Keshavarz, S. Iglauer, *Int. J. Hydrogen Energy* **2011**, *46*, 32809–32845. DOI: https://doi.org/10.1016/j.ijhydene.2021.07.097
[35] A. Azad, M. Duran, *Appl. Catal., A* **2007**, *330*, 77–88. DOI: https://doi.org/10.1016/j.apcata.2007.06.036
[36] R. Chein, Z. Wang, *Int. J. Energy Res.* **2019**, *43*, 3330–3345. DOI: https://doi.org/10.1002/er.4470
[37] A. Salcedo, P. Lustemberg, N. Rui, R. Palomino, Z. Liu, S. Nemsak, S. Senanayake, J. Rodriguez, M. Gauglia-Pirovano, B. L. Irigoyen, *ACS Catal.* **2021**, *11*, 8327–8337. DOI: https://doi.org/10.1021/acscatal.1c01604?rel=cite-as&ref=PDF&jav=VoR
[38] Z. Lian, S. Olanrele, C. Si, M. Yang, B. Li, *J. Phys. Chem. C* **2020**, *124*, 5118–5124. DOI: https://doi.org/10.1021/acs.jpcc.9b09856?ref=pdf
[39] A. Marinho, F. Toniolo, F. Noronha, F. Epron, D. Duprez, N. Bion, *Appl. Catal., B* **2021**, *281*, 119459–119472. DOI: https://doi.org/10.1016/j.apcatb.2020.119459
[40] M. Ouyang, P. Boldrin, R. Maher, X. Cheng, X. Liu, L. Cohen, N. Brandon, *Appl. Catal., B* **2019**, *248*, 332–340. DOI: https://doi.org/10.1016/j.apcatb.2019.02.038
[41] S. Itkulova, G. Zakumbaeva, Y. Nurmakanov, A. Mukazhanova, A. Yermaganbetova, *Catal. Today* **2014**, *228*, 194–198. DOI: https://doi.org/10.1016/j.cattod.2014.01.013
[42] S. Itkulova, Y. Boleubayev, K. Valishevskiy, *J. Sol-Gel Sci. Technol.* **2019**, *92*, 331–341. DOI: https://doi.org/10.1007/s10971-019-05110-3
[43] H. Roh, K. Koo, W. Yoon, *Catal. Today* **2009**, *146*, 71–75. DOI: https://doi.org/10.1016/j.cattod.2009.01.001
[44] P. Phuong, L. Loc, N. Tri, N. Van, N. Ahn, N. Duy, H. Cuong, *Adv. Nat. Sci.: Nanosci. Nanotechnol.* **2020**, *11*, 045013. DOI: https://doi.org/10.1088/2043-6254/abc949
[45] M. Garcia-Dieguez, I. Pieta, M. C. Herrera, M. A. Larrubia, L. J. Alemany, *Catal. Today* **2011**, *172*, 136–142. DOI: https://doi.org/10.1016/j.cattod.2011.02.012
[46] T. Koerts, R. A. van Santen, *J. Chem. Soc. Chem. Commun.* **1991**, *18*, 1281–1283. DOI: https://doi.org/10.1039/c39910001281
[47] J. Guo, H. Lou, X. Zheng, *Carbon* **2007**, *45*, 1314–1321. DOI: https://doi.org/10.1016/j.carbon.2007.01.011
[48] M. Ferrandon, C. Byron, G. Celik, Y. Zhang, C. Ni, J. Sloppy, R. McCormick, K. Booksh, A. Teplyakov, M. Delferro, *Appl. Catal., A* **2022**, *629*, 118379–118397. DOI: https://doi.org/10.1016/j.apcata.2021.118379
[49] P. Frontera, A. Macario, A. Malara, S. Santangelo, C. Triolo, F. Crea, P. Antonucci, *Catalysts* **2018**, *8*, 435–455. DOI: https://doi.org/10.3390/catal8100435
[50] M. Patil, S. Sarris, K. Verbeken, M. Reyniers, K. Geem, *Ind. Eng. Chem. Res.* **2020**, *59*, 15165–15178. DOI: https://doi.org/10.1021/acs.iecr.0c01693
[51] X. Ding, Z. Wang, B. Wang, Z. Xing, *Asia-Pac. J. Chem. Eng.* **2021**, *16*, e2573. DOI: https://doi.org/10.1002/apj.2573
[52] W. Zhang, B. Liu, C. Zhu, Y. Tian, *Appl. Catal., A* **2005**, *292*, 138–143. DOI: https://doi.org/10.1016/j.apcata.2005.05.018
[53] P. Watcher, C. Gaber, J. Raic, M. Demuth, C. Hochenauer, *Int. J. Hydrogen Energy* **2021**, *46*, 3437–3452. DOI: https://doi.org/10.1016/j.ijhydene.2020.10.214

 © 2023 The Authors. Chemical Engineering & Technology published by Wiley-VCH GmbH

15214125, 0, Downloaded from https://onlinelibrary.wiley.com/doi/10.1002/ceat.202200525 by Chua-Consorcio De Bibliotecas, Wiley Online Library on [05/05/2023]. See the Terms and Conditions (https://onlinelibrary.wiley.com/terms-and-conditions) on Wiley Online Library for rules of use; OA articles are governed by the applicable Creative Commons License

Research Article: A catalytic technology to produce H_2 from biogas was investigated. Since biogas is a wet mixture of methane and CO_2, the process currently studied takes advantage of the presence of the two common oxidants used to convert CH_4, an approach often known as bi-reforming of methane. The effect of sulfur, a common poison found in biogas streams, was evaluated by adding dimethyl sulfide to the catalysts.

Bi-reforming of Biogas for Hydrogen Production with Sulfur-Resistant Multimetallic Catalyst

Eduardo Poggio-Fraccari*, Fernando Mariño, Concepción Herrera, María Ángeles Larrubia-Vargas, Luis Alemany

Chem. Eng. Technol. **2023**, *46 (XX)*, XXX … XXX

DOI: 10.1002/ceat.202200525

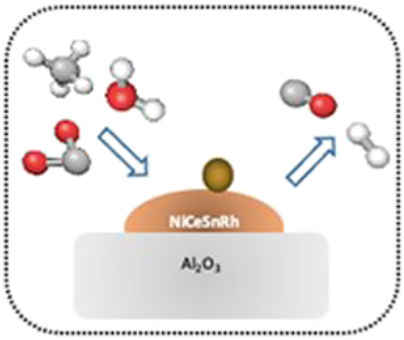

Supporting Information available online

 © 2023 The Authors. Chemical Engineering & Technology published by Wiley-VCH GmbH

15214125, 0, Downloaded from https://onlinelibrary.wiley.com/doi/10.1002/ceat.202200525 by Cbua-Consorcio De Bibliotecas, Wiley Online Library on [05/05/2023]. See the Terms and Conditions (https://onlinelibrary.wiley.com/terms-and-conditions) on Wiley Online Library for rules of use; OA articles are governed by the applicable Creative Commons License